University of Kent

Kent Academic Repository

Oliveira, Ricardo Rodrigues, Molpeceres, Germán, Almeida Silva, Ricardo Montserrat, Fantuzzi, Felipe, Rocha, Alexandre B. and Kästner, Johannes (2023) *Gas-phase C60Hn+q (n = 0–4, q = 0,1) Fullerenes and Fulleranes: Spectroscopic Simulations Shed Light on Cosmic Molecular Structures*. Physical Chemistry Chemical Physics, 25 (37). pp. 25746-25760. ISSN 1463-9076.

Downloaded from

https://kar.kent.ac.uk/102825/ The University of Kent's Academic Repository KAR

The version of record is available from

https://doi.org/10.1039/D3CP03254J

This document version

Author's Accepted Manuscript

DOI for this version

Licence for this version

UNSPECIFIED

Additional information

Versions of research works

Versions of Record

If this version is the version of record, it is the same as the published version available on the publisher's web site. Cite as the published version.

Author Accepted Manuscripts

If this document is identified as the Author Accepted Manuscript it is the version after peer review but before type setting, copy editing or publisher branding. Cite as Surname, Initial. (Year) 'Title of article'. To be published in ***Title of Journal*** , Volume and issue numbers [peer-reviewed accepted version]. Available at: DOI or URL (Accessed: date).

Enquiries

If you have questions about this document contact ResearchSupport@kent.ac.uk. Please include the URL of the record in KAR. If you believe that your, or a third party's rights have been compromised through this document please see our Take Down policy (available from https://www.kent.ac.uk/guides/kar-the-kent-academic-repository#policies).

PCCP

Gas-phase C60Hn+q (n = 0–4, q = 0,1) Fullerenes and Fulleranes: Spectroscopic Simulations Shed Light on Cosmic Molecular Structures

Journal:	*Physical Chemistry Chemical Physics*
Manuscript ID	CP-ART-07-2023-003254.R1
Article Type:	Paper
Date Submitted by the Author:	31-Aug-2023

Complete List of Authors:	Oliveira, Ricardo; Federal University of Rio de Janeiro, Physical Chemistry Molpeceres, Germán; The University of Tokyo, Department of Astronomy Almeida Silva, Ricardo Montserrat; Federal University of Rio de Janeiro, Fantuzzi, Felipe; University of Kent, School of Chemistry and Forensic Science Rocha, Alexandre; Federal University of Rio de Janeiro, Physical Chemistry Kästner, Johannes; University of Stuttgart, Institute for Theoretical Chemistry

SCHOLARONE™
Manuscripts

PCCP

ARTICLE TYPE

Cite this: DOI: 00.0000/xxxxxxxxxx

Gas-phase $C_{60}H_n^{+q}$ (n = 0–4, q = 0,1) Fullerenes and Fulleranes: Spectroscopic Simulations Shed Light on Cosmic Molecular Structures

Ricardo R. Oliveira,*[a] Germán Molpeceres,*[b] Ricardo Montserrat,[a] Felipe Fantuzzi,[c] Alexandre B. Rocha[a] and Johannes Kästner.[d]

Received Date
Accepted Date

DOI: 00.0000/xxxxxxxxxx

The discovery of C_{60}, C_{60}^+, and C_{70} in the interstellar medium has ignited a profound interest in the astrochemistry of fullerene and related systems. In particular, the presence of diffuse interstellar bands and their association with C_{60}^+ has led to the hypothesis that hydrogenated derivatives, known as fulleranes, may also exist in the interstellar medium and contribute to these bands. In this study, we systematically investigated the structural and spectroscopic properties of $C_{60}H_n^{+q}$ (n = 0-4, q = 0,1) using an automated global minimum search and density functional theory calculations. Our results revealed novel global minimum structures for $C_{60}H_2$ and $C_{60}H_4$, distinct from previous reports. Notably, all hydrogenated fullerenes exhibited lower ionization potentials and higher proton affinities compared to C_{60}. From an astrochemical perspective, our results exposed the challenges in establishing definitive spectroscopic criteria for detecting fulleranes using mid-infrared and UV-Vis spectroscopies. However, we successfully identified distinct electronic transitions in the near-infrared range that serve as distinctive signatures of cationic fulleranes. We strongly advocate for further high-resolution experimental studies to fully explore the potential of these transitions for the interstellar detection of fulleranes.

1 Introduction

Today, there is a consensus that carbonaceous materials of medium to large size (10–100 atoms) are the leading carriers of the enigmatic spectral features known as diffuse interstellar bands (DIBs).[1–3] These bands, known since the early 1920s,[4] have posed a significant puzzle to observational astronomy ever since. In addition to the puzzling existence of these molecular lines, we encounter further conundrums, such as the fraction of atomic carbon confined within intricate molecular structures, including polycyclic aromatic hydrocarbons (PAHs), graphene, graphite, or the main family of compounds of interest in this work, fullerenes. In fact, it is estimated that ca. 10% of the total interstellar carbon is locked in these classes of molecules, as inferred from their infrared emission (see Table 12.3 in Tielens 2021).[5] From a physicochemical point of view, the prevalence of carbon-bearing molecules made up of condensed aromatic rings finds its origin in their resilience against photofragmentation. Larger PAHs, for instance, exhibit a higher resistance to photofragmentation compared to photoionization, thus underscoring the correlation between PAH size and stability.[6] Indeed, a possible explanation for the formation of fullerenes in space revolves around the successive photoisomerization of large PAHs.[7,8] Additionally, high-temperature condensation of PAHs represents another mechanism implicated in the production of fullerenes.[9] These findings pose a series of requirements that molecules must meet to be detectable within photodissociation regions (PDRs).

The presence of buckminsterfullerene (C_{60}) in the interstellar medium (ISM) was inferred by detection of two distinct absorption features attributed to its ionized species (C_{60}^+), at 9632 Å and 9577Å,[10] in the characteristic region of DIBs. Furthermore, the detection of C_{60} has also been reported in planetary nebulae.[11] The ionization potential (IP) of C_{60} , which is 7.61 eV,[12] falls below the Lyman limit of 13.6 eV. This implies that in PDRs, the preferred form of C_{60} is its ionized state, C_{60}^+. From a chemical point of view, C_{60}^+ is highly reactive radical

[a] Chemistry Institute, Federal University of Rio de Janeiro, Rio de Janeiro, Brazil.
[b] Department of Astronomy, Graduate School of Science, The University of Tokyo, Tokyo 113 0033, Japan
[c] School of Chemistry and Forensic Science, University of Kent, Canterbury CT2 7NH, UK.
[d] Institute for Theoretical Chemistry, University of Stuttgart, Stuttgart, Germany.
*Corresponding authors. Mail addresses: rrodrigues.iq@gmail.com, molpeceres@astron.s.u-tokyo.ac.jp

† Electronic Supplementary Information (ESI) available: High-resolution figures of the structures, spectroscopy of C_{60}, C_{60}^+, $C_{60}H$ and $C_{60}H^+$, spectra in the C–H stretching region, benchmarks and detailed numerical values of enthalpies, electronic transitions' oscillator strengths and ionization potentials.

cation, readily engaging in reactions with both radical and neutral species without the need for activation barriers.[13–15] In PDRs, the most abundant species is atomic hydrogen, H.[1] Therefore, C_{60}^+ is expected to experience hydrogenation in these regions. Following a cycle of hydrogenation and ionization, subsequent additions of H can be favored, leading to $C_{60}H_n^{+q}$ species. In the gas phase, the release of chemical energy in exothermic reactions can significantly influence the subsequent reaction pathway. In the case of cationic carbon cages like C_{60}^+, addition reactions are preferred for two main reasons. Firstly, the ionized state of the system enhances its reactivity propensity, as mentioned earlier. Secondly, addition reactions contribute to the alleviation of strain energy in the carbon cage through the formation of covalent bonds with the added species.[16]

Based on the aforementioned reasons, it is anticipated that the addition of hydrogen atoms to C_{60} and C_{60}^+ plays a significant role in interstellar chemistry. These reactions would result in the formation of hydrogenated fullerenes of formula $C_{60}H_n^{+q}$, namely fulleranes. These species are susceptible to astronomical detection, as demonstrated by Iglesias-Groth *et al.*[17]. Furthermore, the hydrogenated fullerenes can act as reservoirs for hydrogen atoms, similar to PAHs, contributing to the formation of H_2 in interstellar environments, as supported by previous studies.[18–22] Our goal is to investigate the main hydrogenation channels of $C_{60}H_n^{+q}$. However, exploring the chemical space of the different hydrogenation channels is very challenging due to the exponential growth of possible combinations, resulting from the appearance of competitive hydrogenation pathways. Previous research by Zhang and co-workers[23], focused on the theoretical study of neutral $C_{60}H_n$ fulleranes, especifically for even values of n up to 60 and $q = 0$, and included the analysis of their infrared spectra. Additionally, several efforts on synthesis and characterization were done focused on $C_{60}H_2$ and $C_{60}H_4$ fulleranes.[24–30] Furthermore, a recent successful and facile bottom-up synthesis of $C_{40}H_{10}$ from benzocorannulene, a structural isomer of coronene,[31] further emphasizes the significance of fulleranes in the astrochemical context.

In this work, we expand on the works of Zhang and coworkers,[23] focusing on the characterization of low-lying isomers of $C_{60}H_n^{+q}$ for n = 0–4 and q = 0,1 using first-principles simulations in combination with recently developed automated conformer search engines based on the extended tight-binding method.[32] Similar methods were applied in the study of hydrogenation of small carbon cages.[33] To contribute to our ulterior goal of proposing new $C_{60}H_n^{+q}$ candidates for astronomical detection, we have derived spectroscopic data in the ultraviolet (UV) and infrared (IR) regions. These data hold the potential to assist in future astronomical searches, including those conducted with advanced instruments like the James Webb Space Telescope (JWST). To ensure the reliability of our theoretical investigations, we have benchmarked our data against experimental results whenever available. Furthermore, we have identified the most promising H-bearing derivatives of C_{60}, which exhibited significant potential in the chemical processes involved in the interstellar formation of H_2 from C_{60}. The paper is organized as follows: In Section 2 we present our computational approach to the project. In Section 3.1 we describe the notation and the main structures of of $C_{60}H_n^{+q}$. This is followed by Section 3.2 where we present the main findings on the low-lying isomers of $C_{60}H_n^{+q}$, including their infrared spectral features. In Section 3.3 we discuss the absorption electronic spectra with special focus on the low-energy transitions. Lastly, in Section 3.4, we synthesize our findings and provide a comprehensive analysis of their implications within the context of interstellar chemistry.

Table 1 Ionization potential (IP) and proton affinities (PA) for all global minimum neutral species considered in this work obtained with B3LYP-D3/def2-TZVP level of theory. In parenthesis, experimental values from the literature.

Species	IP (eV)	PA (kJ mol^{-1})
C_{60}	7.33 (7.61)[a]	864 (853-866)[b]
$C_{60}H$	6.60	946
$C_{60}H_2$	7.03	889
$C_{60}H_3$	6.40	915
$C_{60}H_4$	6.81	-

[a] As reported by Lichtenberger and co-workers[12]
[b] As reported by McElvany and co-workers[51]

2 Computational details

The starting geometries of C_{60} and C_{60}^+ (D_{5d}) were obtained from the works of Schwerdtfeger *et al.*[34] and Lykhin*et al.*[35], respectively. Then, geometry optimization and Hessian computations were performed applying density functional theory (DFT) with the B3LYP-D3[36–39] hybrid functional combined with the def2-TZVP basis set.[40] Furthermore, we conducted benchmark computations using time-dependent density functional theory (TDDFT) with the PBE0,[41,42] CAM-B3LYP[43] and ωB97X-D3[44] hybrid functionals, and revTPSS[45] and r^{2}SCAN[46] within meta-generalized gradient approximation (meta-GGA). The results are present in the Supporting Information (SI), from which the r^{2}SCAN functional[46] was selected because it was the functional that managed to reproduce the absorption bands in the fullerene spectrum. Infrared spectra were simulated at the B3LYP-D3/def2-TZVP level and uncertainties on the wavenumbers are in between 10 cm^{-1} and 15 cm^{-1}.[47]. Electronic absorption spectra (EAS) were obtained at r^{2}SCAN/def2-TZVP level, with an estimated uncertainty around 0.3 eV and 0.6 eV for vertical transition energies.[48,49] A Lorentzian fit with full width at half maximum (FWHM) of 10 cm^{-1} was applied for the IR spectra simulations, while for EAS a Gaussian function with FWHM of 15 nm was used. A scaling factor of 0.9671 was applied[50] to the IR wave numbers to take into account the anharmonic effects.

Neutral ($q = 0$) and cations ($q = +1$) of $C_{60}H_n$ were obtained applying the tautomerization routine for the prediction of (de)protonation sites[32,52,53] implemented in the extended tight binding (xtb) program package through the Conformer-Rotamer Ensemble Sampling Tool (CREST) based code.[54] In this step, the GFN2-xTB method was applied.[55] To select $C_{60}H$ and $C_{60}H_2$ isomers, an energy threshold of 60 kcal mol^{-1} was considered and the final geometries were reoptimized using the PBEh-3c composite method.[56] Due to computational limitations, smaller en-

Table 2 Dipole moment (μ) and carbon−hydrogen distances ($\bar{r}_{C-H}$) for all species considered in this work obtained with B3LYP-D3/def2-TZVP level of theory.

Species	$\bar{r}_{C-H}$ (Å)		μ (Debye)	
	$q=0$	$q=+1$	$q=0$	$q=+1$
C_{60}	-	-	0.00	0.00
$C_{60}H$	1.099	1.101	1.51	3.55
$C_{60}H_2$	1.093	1.094	2.61	3.56
$C_{60}H_3$	1.093	1.097	3.55	5.56
$C_{60}H_4$	1.093	1.093	2.77	3.71

ergy thresholds were applied for $C_{60}H_n$ ($n=3,4$). For the $C_{60}H_3$ search, the lowest four energy structures from $C_{60}H_2$ were considered as input structures and the energy threshold was set to 30 kcal mol^{-1}. In turn, for the the $C_{60}H_4$ system, the lowest ten energy structures from $C_{60}H_3$ were used as input geometries and the energy threshold was established between 20 and 30 kcal mol^{-1}. All geometries selected from the CREST code were optimized at the PBEh-3c level and further (re)optimized at the B3LYP-D3/def2-TZVP level of theory. For the TDDFT computations, the r^{2}SCAN/def2-TZVP level was used in the B3LYP-D3/def2-TZVP geometries. We used 300 electronic states in this step.

The IPs were computed by the following equation:

$$IP = U^0_{\mathrm{mol}^+} - U^0_{\mathrm{mol}} \quad (1)$$

where U^0_{mol} and $U^0_{\mathrm{mol}^+}$ are the internal energies at 0 K of the neutral and cationic structures, respectively. In turn, proton affinities (PAs) are given by:

$$PA = (H^\circ_{\mathrm{mol}} + H^\circ_{\mathrm{H}^+}) - H^\circ_{\mathrm{mol\text{-}H}^+} \quad (2)$$

where H°_{mol} is the standard enthalpy of the molecular (*mol*) species and $H^\circ_{\mathrm{H}^+}$ is the proton enthalpy at 298.15 K (6.14 kJ mol^{-1}) taken from the literature.[57] This computational approach was previously applied in the study of polycyclic aromatic phosphorus heterocycles (PAPHs).[58] All DFT and xtb calculations were performed using the ORCA 5.0[59] and xTB 6.4 software packages, respectively.

3 Results and discussion

3.1 Notation, molecular structures and relative enthalpies

We used a notation of the form **Nz** for neutrals and **Nz-c** for cations. The "**N**" represents the number of hydrogen atoms and the letter "**z**" represents the energetic (final) order (**a** for the first isomer, **b** for the second, ...). For the cations, we added the letter "**c**" indicating the charge state of the cation. In Figure 1, all low-energy structures obtained from the automated script using the CREST tool after optimization at the B3LYP-D3/def2-TZVP level of theory are presented. The numbers below each structure label are the relative enthalpies for a given molecular series, i.e., for a specific **N** and charge state. A larger version of this figure can be found in the SI (Figures S1 to S5). The relative enthalpies for low-energy isomers can also be found in the SI (Tables S1, S2, and S3).

It is important to note that in the mentioned tables and Figure 1 there is an additional notation, **Nz**$^+$. This notation signifies that **Nz**$^+$ species was obtained using the **Nz** optimized geometry. For instance, in Table S1 we indicated that **2a-c** ($C_{60}H_2^+$ global minimum) is identical to **2a**$^+$ (cation from **2a**). On the other hand, **2c-c** is derived from the ionization of **2d** (which we also referred as **2d**$^+$). Also, ZGM stands for Zhang's global minimum.

3.2 Structural features, properties and simulated infrared spectra

The simulated IR spectrum of C_{60} is shown in Figure S6 (top left panel). The scaling factor of 0.9671 was applied[50] for a better comparison with the experimental spectrum. A good agreement was obtained; the four bands (A: 526 cm^{-1}, B: 576 cm^{-1}, C: 1182 cm^{-1}, and D: 1428 cm^{-1}) that represent the normal modes T_{1u} (IR active) were reproduced.[60] Also, our results are very close to previously reported DFT simulations.[61,62] Furthermore, the IP computed at the B3LYP-D3/def2-TZVP level is 7.33 eV (Table 1), close to the experimental value of 7.61 eV.[12] In the cationic state (C_{60}^+), fullerene exhibits a Jahn-Teller distortion making the isomer with D_{5d} symmetry the global minimum.[35] Consequently, due to the symmetry reduction, more normal modes are IR active. In Figure S6 (bottom left panel), a comparison between our result and the experimental one is presented with reasonable agreement.[63,64]

The C_{60} theoretical PA of 864 kJ mol^{-1} (Table 1) is within the range of experimental measurements (853 – 866 kJ mol^{-1}).[51] The protonation process strongly reduces the C_{60} symmetry and consequently, the IR spectrum of $C_{60}H^+$ is more complex than the spectra of C_{60} and C_{60}^+ (Figure S6, right panels). Endohedral protonation is unlikely to occur, as already demonstrated, i.e., only the exohedrally protonated isomer should be formed.[62]

As pointed out earlier by Palotás and co-workers,[62] the $C_{60}H^+$ spectrum has intense bands in the range of 1150–1570 cm^{-1} (6.4–8.7 μm) and the main contributions are C–C stretching and C–C–H bending modes. The intense band around 1400 cm^{-1} is also present in the C_{60} and C_{60}^+ spectra. Furthermore, there are two strong bands around 525 and 565 cm^{-1} (19.1 and 17.7 μm) that are present again in the C_{60} and C_{60}^+ spectra. However, the relative intensity is weaker than that of the neutral and stronger than that of the cation fullerene bands. The cage (skeleton) deformation modes are present in 760 and 955 cm^{-1} (13.15 and 10.45 μm) but are relatively weak. The single C–H stretching mode was not revealed experimentally, but for solid hydrogenated fullerenes[65] this band is present around 2900 cm^{-1} (3.44 μm) and our (scaled) result is 2870 cm^{-1} (3.48 μm); see Figure S9. This discrepancy is due to the high anharmonicity in the hydrogen stretching region. Concerning the IR spectrum of the neutral single hydrogenated species, $C_{60}H$, in contrast to the case of the cation, only one strong band is present above 1200 cm^{-1} around 1400 cm^{-1} (7.14 μm). In addition, the two intense bands below 600 cm^{-1}, centered around 585 cm^{-1} (17.09 μm) and 530 cm^{-1} (18.86 μm), are more intense than the ones in the cation IR spectrum. However, the C–H stretching mode exhibits

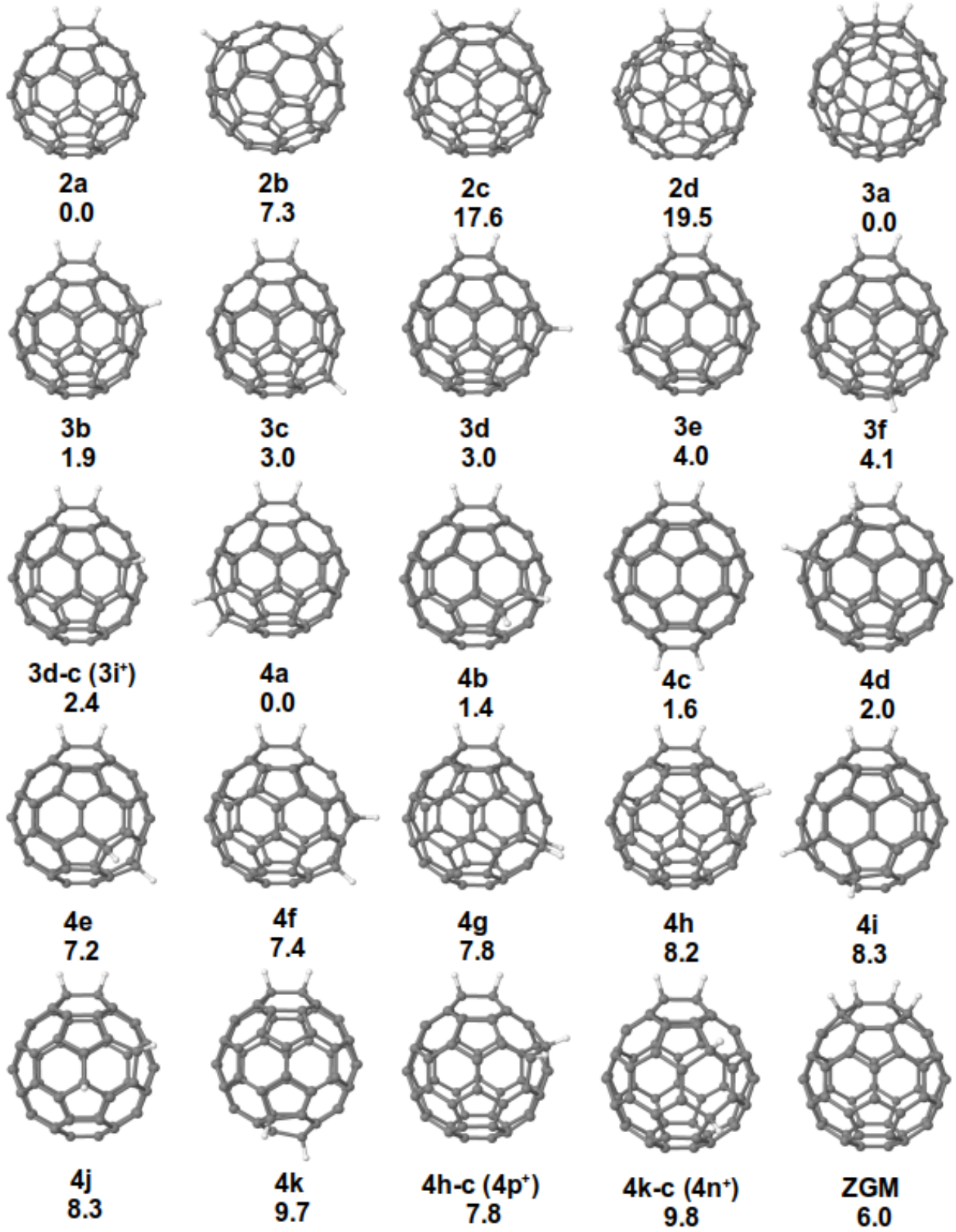

Fig. 1 Molecular structure of all species studied in this work. The label beneath each structure represents its identification, while the number indicates the enthalpy in kcal mol^{-1} relative to the corresponding global minimum energy structure. Carbon: gray. Hydrogen: white.

the same wavenumber but lower intensity, probably due to the difference in the dipole moments from 1.51 to 3.55 D for $C_{60}H$ and $C_{60}H^+$, respectively. The C–H distance ($\bar{r}_{C-H}$) was unaffected (see Table 2) and its ionization potential of 6.60 eV (see Table 1)

is smaller than that of C_{60}.

There are several hydrogenation pathways to form $C_{60}H_2$ systems ($n = 2$). We found a global minimum (**2a**) with two vicinal hydrogen atoms in between two six-membered rings (naphthalene-like unit); see Figure S1 in the SI. The second isomer in energy (**2b**) is 7.29 kcal mol^{-1} above **2a**. The third (**2c**) and forth **2d** structures are high-energy isomers with relative energies of 17.6 and 19.5 kcal mol^{-1}, respectively (Table S1). In terms of the IR spectra in Figure 2, **2a** and **2b** have similar profiles compared to $C_{60}H$ while **2c** and **2d** have more complex patterns, especially in the region between 600 cm^{-1} and 1000 cm^{-1} where some intense bands are present due to skeleton distortion and C–C–H bending modes. The C–H distance value of $\bar{r}_{C-H}$ = 1.093 Å in **2a** is very close to the $C_{60}H$ case but the dipole moment and IP are higher, 2.61 D (Table 2) and 7.03 eV (Table 1), respectively. It is worth noting that the **2a** isomer was not reported by Zhang et al.[23] The lowest energy isomer reported by them was **2c** and the simulated IR spectra are in reasonable agreement with ours. The IPs for all low-energy isomers are presented in Table S9. The mean values are very close to the IP of the global minimum structures.

The PA of $C_{60}H$ forming **2a-c** is higher than C_{60} which indicate that $C_{60}H_2^+$ can be formed if H^+ and $C_{60}H$ are available. This structure is the $C_{60}H_2^+$ global minimum and it is similar to that of **2a**. Consequently, we can refer to **2a-c** also as **2a**$^+$. Both are presented in Table S1 for all reported $C_{60}H_2^+$ isomers. Furthermore, the dipole moment and distances $\bar{r}_{C-H}$ are very close to the $C_{60}H^+$ values. The second isomer in energy is **2b-c** (or **2b**$^+$) and is 7.52 kcal mol^{-1} above **2a-c**. The next two isomers are **2c-c** (**2d**$^+$) and **2d-c** (**2c**$^+$) are 10.01 and 11.81 kcal mol^{-1} above **2a-c**. Note that in Table S1 the energy differences between the cations are smaller than the neutral ones.

In the IR spectra of **2a-c**, intense bands around 1530, 1390 and 1180 cm^{-1} (6.53, 7.19 and 8.47 μm) are present with the main contribution from C–C stretching modes. At 1162 cm^{-1} (8.60 μm), the bending mode C–C–H represents the most intense band in this spectrum. The C–H stretching mode appears at 2939 cm^{-1} (3.40 μm). In the next isomer (**2b-c**) spectrum, the band around 1530 cm^{-1} has lower intensity compared to **2a-c** and there is a band splitting around 1400 cm^{-1}. The most intense band in this case was centered at 1153 cm^{-1} (8.67 μm) due to the C–C stretching and C–C–H bending modes. A small redshift of 39 cm^{-1} in the C–H stretching mode was obtained. The most prominent features in the IR spectra of **2c-c** and **2d-c** are the intensity increase in the C–C stretching (1300–1600 cm^{-1}) and skeleton (400–600 cm^{-1}) distortion regions when compared to the **2a-c** and **2b-c** ones. The C–H stretching mode for all $C_{60}H_2$ isomers (neutral and cation charge states) appears in between 3.4–3.5 μm (2941–2857 cm^{-1}), see Figure S10.

The global minimum (**3a**) of $C_{60}H_3$ ($n = 3$) has three neighboring hydrogen atoms. Our results suggest that all low energy isomers (from **3b** to **3f**) in Figure S2 can be formed from the **2a** + H reaction. The energy differences in this family ($n = 3$) are lower than those of $n = 2$. The relative energies (Table S2) are 1.9, 3.0, 3.0, 4.0 and 4.1 kcal mol^{-1} for **3b**, **3c**, **3d**, **3e** and **3f**, respectively. The IP of **3b** that forms the global minimum cation, **3a-c** (**3b**$^+$) is 6.40 eV. The distances between C and H are equal to $C_{60}H_2$ ($\bar{r}_{C-H}$ = 1.093 Å) and the proton affinity of **2a** forming **3a-c** is 889 kJ mol^{-1} (Table 1).

The next isomer (**3b-c**) is equivalent to **3a**$^+$, which is only 0.43 kcal mol^{-1} higher in energy compared to **3a-c**. Again, the differences in energy are smaller for the cation isomers (see Table S2). Also, the fourth structure, **3d-c**, is formed from the ionization process of the ninth neutral isomer, **3i**. The $\bar{r}_{C-H}$ values were very similar to the $n = 2$ case, but the dipole moments are higher, 3.55 and 5.56 Debye for the neutral and cation, respectively (Table 2). The spectroscopic profiles are very similar to the $C_{60}H_2$ case, exhibiting intense bands near 600 cm^{-1} (skeleton distortion) and 1400 cm^{-1} (C–C stretching), as can be seen in Figure 3. Moreover, small differences can be pointed out. In the **3b** spectrum, the band between 400 cm^{-1} and 600 cm^{-1} has three peaks instead of two, and the one around 1400 cm^{-1} was split into two peaks. The same is true for the cation spectra, but in this case, the high-intensity bands between 1100 and 1600 cm^{-1} (Figure 3), in which the main contributions are C–C stretching and C–C–H bending modes, have small differences, such as the number of peaks and relative intensities. In the C–H stretching region, **3a** has three bands centered at 2890, 2915 and 2959 cm^{-1} (3.46, 3.43 and 3.37 μm) while **3a-c** has a band at 2877 cm^{-1} (3.47 μm). In general, $C_{60}H_3$ infrared spectra have more bands than $C_{60}H_3^+$ related to C–H stretching modes, as can be seen in Figure S11.

Taking into account the $C_{60}H_4$ system, several low-lying energy isomers were obtained. It is worth mentioning that the global minimum (**4a**) can be formed from hydrogen addition to **3c** instead of **3a**. Also, Zhang's global minimum (ZGM)[23] structure was not found during our global search. Nevertheless, we considered this structure and the related cation and computed the total energies and Hessians. The ZGM is above **4a** by 6.0 kcal mol^{-1}, indicating that we found a new GM for the $C_{60}H_4$ system. Furthermore, none of the low energy isomers (from **4b** to **4k**) can be formed from **3a**, revealing complex reaction branches for synthesizing highly hydrogenated fullerenes. Structures from **4a** to **4c** exhibit two groups of vicinal hydrogen atoms, and the latter two are 1.4 and 1.6 kcal mol^{-1} above the global minimum. The cation global minimum, **4a-c** (equivalent to **4a**$^+$), can be formed from the ionization of **4a** which has an ionization potential of 6.81 eV, slightly higher than **3a**. The C–H distances ($\bar{r}_{C-H}$) in **4a** and **4a-c** are equal to the **3a** distance, 1.093 Å. However, the dipole moments are smaller than the $n = 3$ ones, which are 2.77 and 3.71 Debye for the neutral and the cation, respectively (see Table 2). **4b-c** is very close in energy to **4a-c**, only 0.42 kcal mol^{-1}, indicating a competition for the global minimum position (see Table S3).

In general, the IR spectra of $C_{60}H_4$ exhibits an intensity decrease of the band around 1400 cm^{-1} (C–C stretching region); see Figure 4. An intense band related to the C–H stretching mode appears at 2942 cm^{-1} (3.39 μm) in the **4a** spectrum. Also, **4h** exhibits a similar IR spectrum to **3b** probably due to geometric similarities, and **4h** can be formed from "**3b** + H" reaction. In the cation IR spectrum of **4a-c** in Figure 5, a difference can be seen in the bands between 1100 and 1600 cm^{-1} (C–C stretching and

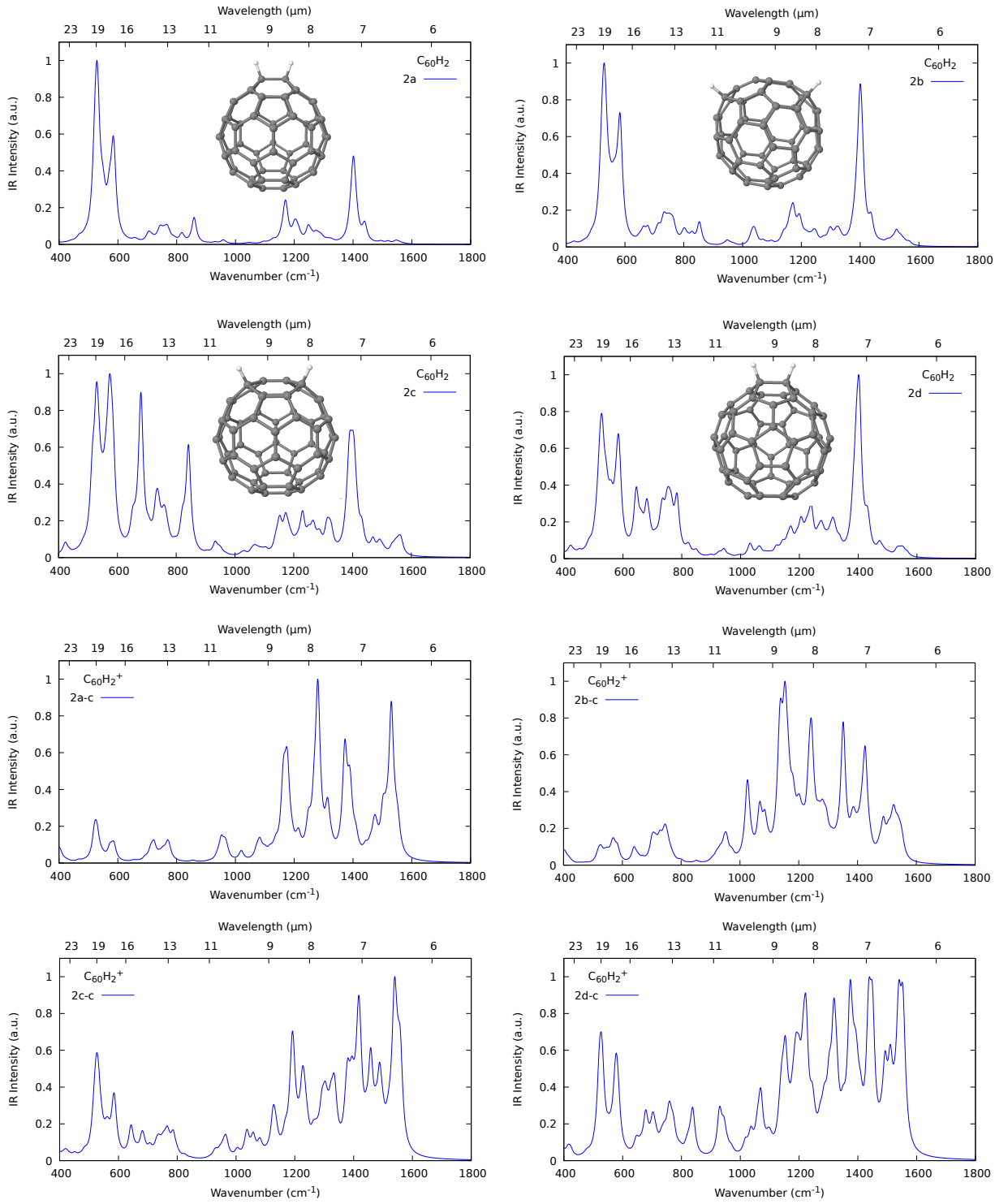

Fig. 2 Simulated infrared spectra of $C_{60}H_2$ and $C_{60}H_2^+$ at the B3LYP-D3/def2-TZVP level of theory.

C–C–H bending region) compared to the $n = 2$, 3 cations. Three groups of bands have a progressive increase in intensity, but, in general, a complex intensity pattern is noticed for most cation isomers with $n = 3$, 4 (see Figures 3 and 5). Again, for the cation global minimum (**4a-c**) the most intense band in the C–H stretching region is located at 2942 cm^{-1} (3.39 μm). For the $C_{60}H_4$ at neutral charge states, the C–H stretching bands are more intense than the cation ones; see Figures S12 and S13. Also, for neutral species, several IR spectra exhibit double band between 3.4–3.5 μm (2941–2857 cm^{-1}).

For the open shell systems, we found that IPs are smaller and PAs are higher, *i.e.*, for $C_{60}H$ and 3a molecules. Also, the dipole

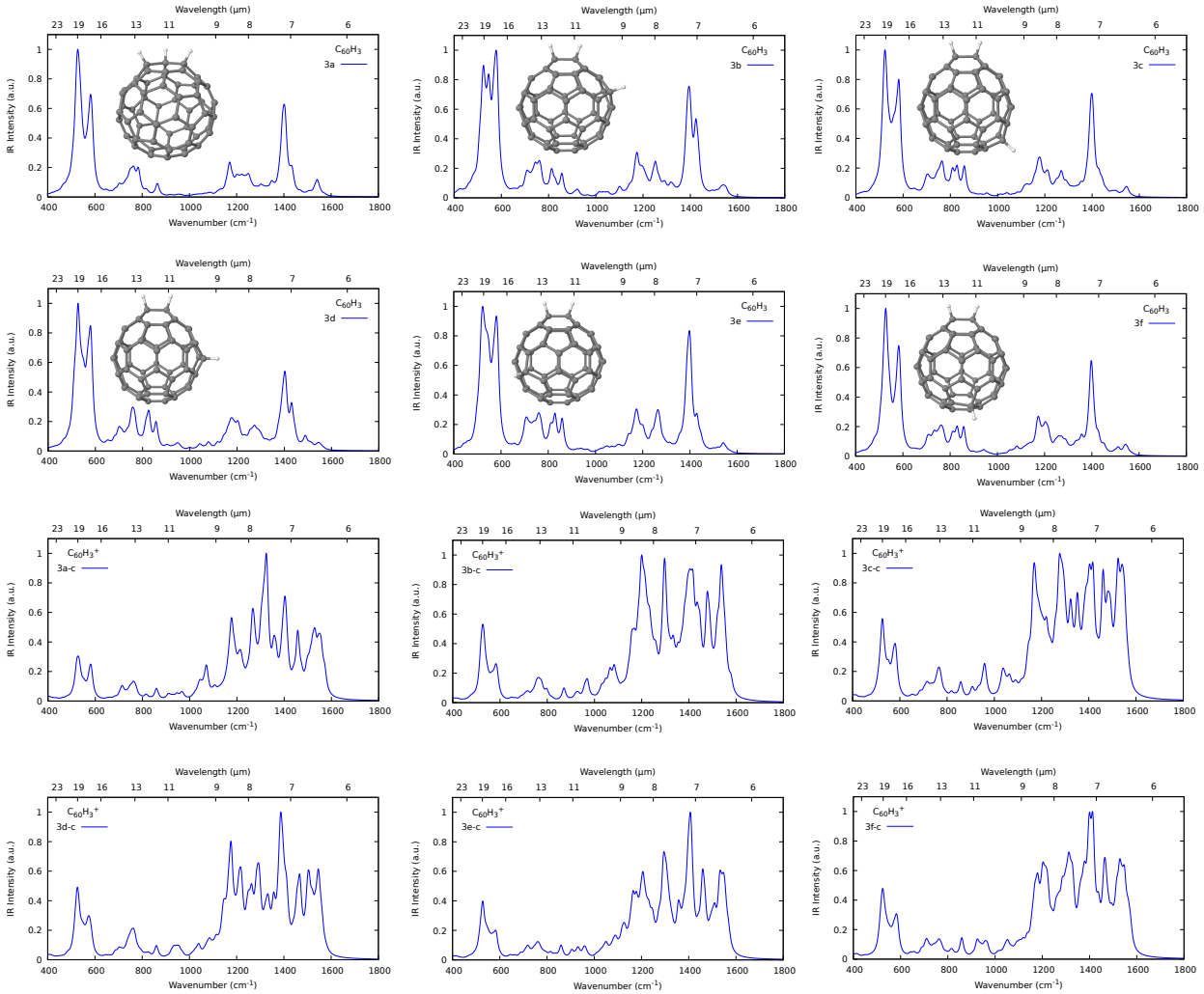

Fig. 3 Simulated infrared spectra of $C_{60}H_3$ and $C_{60}H_3^+$ at the B3LYP-D3/def2-TZVP level of theory.

moments are higher for the $C_{60}H_3$ species due to the hydrogen atoms proximity inducing a structural cage distortion in the same region and, consequently, increasing the dipole moments of **3a** and **3a-c**. Moreover, an overall trend for spectroscopic properties was not obtained probably due to the limited number of hydrogenated species studied in this work. The trends are present in Figures S15, S16 and S17.

The trends for the IR spectra are, for neutral species there are intense bands around 500-600 cm^{-1} (20.00-16.66 μm) due to skeleton (delocalized) deformation normal modes. However, the cation spectra exhibit intense bands in the range of 1200-1600 cm^{-1} (8.33-6.25 μm), related to C–C stretching and C–C–H bending (localized) normal modes. A possible explanation is, for the cations (protonated species), the dipole moments are higher indicating a more distorted carbon cage structure. Consequently, several C–C stretching and C–C–H bending modes will further increase the dipole along the normal mode resulting in an intensity enhancement of the bands in the 1200-1600 cm^{-1} region.

3.3 Electronic transitions

The simulations of the electronic spectra of C_{60} are shown in Figure S7. From the experimental results, the allowed transitions were obtained in the 190 nm – 410 nm wavelength range and were characterized as $^1A_g \longrightarrow {}^1T_{1u}$.[66] Transitions with very low intensities were also obtained between 410 nm and 620 nm due to vibronic coupling through Jahn-Teller distortions.[66] The three main bands in the experimental spectrum were well reproduced with r^{2}SCAN and revTPSS but with hybrid functionals the agreement is very poor, revealing that meta-GGA are a suitable choice for electronic spectra simulations of fullerenes. The best result was obtained with r^{2}SCAN and, consequently, all results reported from now on were obtained with this functional. It is important to note that the vertical energy transitions are very close to the experimental results, in which the higher deviation is about 0.06 eV (see Table S4).

In the case of fullerene cation (C_{60}^+), the Jahn-Teller coupling is even more important because of low-energy isomers with different symmetries. The C_{60}^+ vertical transitions were obtained with the global minimum structure which has D_{5d} symmetry and they

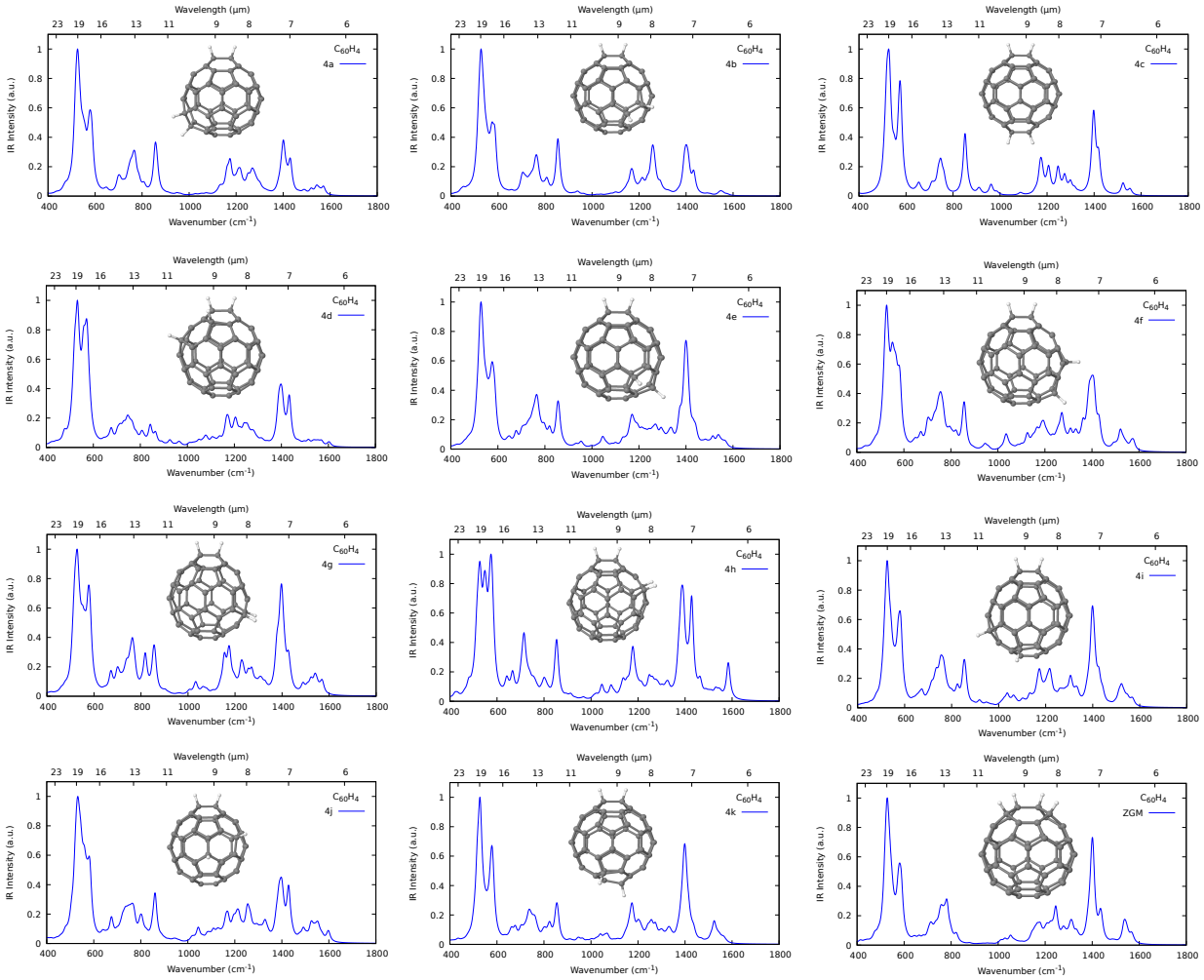

Fig. 4 Simulated infrared spectra of $C_{60}H_4$ at the B3LYP-D3/def2-TZVP level of theory.

are shown in Table S4. Lykhin *et al.* performed a detailed simulation of the lowest electronic transitions of C_{60}^+.[35] The authors demonstrated that the strong DIBs at 9632 and 9577 Å are due to the Jahn–Teller split of the lowest E_{1g} excited state. Also, the weak DIBs at 9428 Å and 9365 Å are due to vibronic coupling. Indeed, the vibronic coupling is also important, as highlighted in the work by Soler and collaborators.[67] The vertical transitions (obtained with TDDFT) from the global minimum (D_{5d}) with larger oscillator strengths are around 892 and 801 nm. However, the vibronic coupling effect makes the bandwidth larger, reaching around 1000 nm. Our results obtained with r^{2}SCAN are in good agreement with the vertical transitions previously reported (Table S4).[35,67] In this case the main vertical transitions obtained in this work have a higher deviation of 0.04 eV, which is very small.

The electronic transitions of $C_{60}H$ and $C_{60}H^+$ are shown in Figure S8. These structures show maxima between 200 nm and 300 nm, as well as the other protonated molecules shown below. However, it should be noted that the electronic transitions for $C_{60}H$ and $C_{60}H^+$ begin in the near-IR region. Thus, an inset highlighting the spectrum above 850 nm is also reported for each system. This procedure is repeated for all the spectra that exhibit transitions in the near-IR. Both $C_{60}H$ and $C_{60}H^+$ exhibit large redshifts in the energies of the first excitations compared to C_{60} and C_{60}^+. The first four transitions of the cation ($C_{60}H^+$) are slightly shifted to smaller energies compared to $C_{60}H$. On the other hand, two additional transitions are observed for $C_{60}H$ above 900 nm.

None of the observed transitions for **2a** and **2b** are in the near-IR region (Figure 6). Nevertheless, the simulated **2a** EAS is in good agreement with available experimental data reproducing the band around 250 nm (see Figure S14).[24–27] Still, the **2c** and **2d** isomers show one and two excitations, respectively, in this region of the spectrum. Similarly to the results discussed previously, the cations present redshifts compared to the neutral counterparts. The **2a-c** and **2b-c** cations have weak transitions occurring up to very high wavelengths of 3832 nm (0.32 eV) and 4429 nm (0.28 eV), respectively. Furthermore, these species show other bands below 900 nm. **2c-c** and **2d-c** isomers also exhibit several transitions in this range. However, these ionized molecules present the first bands up to ca. 2000 nm (0.62 eV).

Interestingly, neutral fullerenes containing three hydrogen atoms ($C_{60}H_3$) show the low-energy region of the spectra varying between 1250 nm (0.99 eV) and 1150 nm (1.08 eV). Figure 7

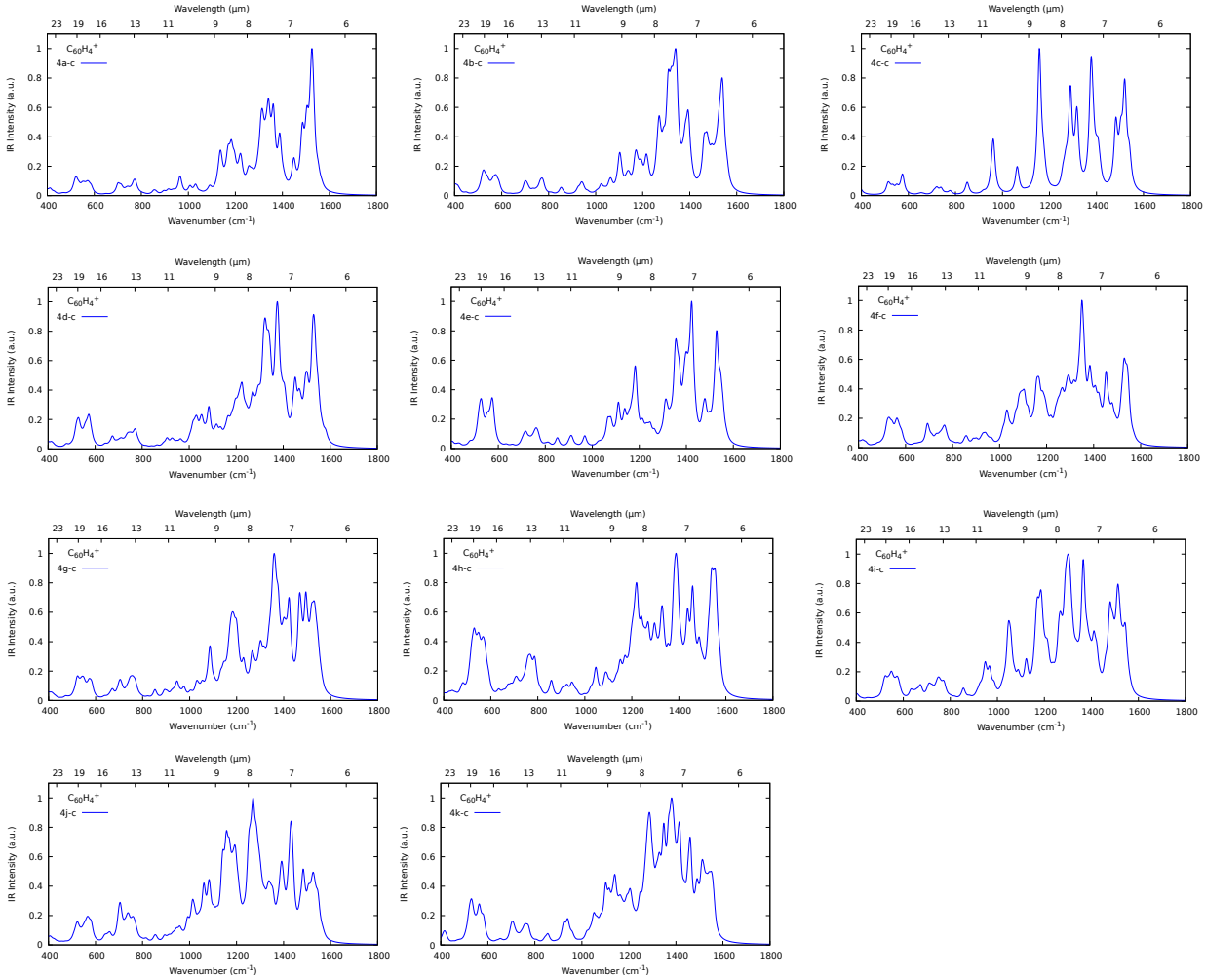

Fig. 5 Simulated infrared spectra of $C_{60}H_4^+$ at the B3LYP-D3/def2-TZVP level of theory.

shows that these values are red-shifted compared to species with one and two hydrogen atoms in the structures as shown previously. However, the first excitations of the cations ($C_{60}H_3^+$) exhibit higher energies compared to the $C_{60}H_2^+$ species. The cations show transitions with wavelengths longer than those of the neutral analogs, which is a pattern also seen in the $C_{60}H$ and $C_{60}H_2$ systems.

The electronic absorption spectra for the $C_{60}H_4$ isomers and their cations ($C_{60}H_4^+$) are shown in Figures 8 and 9, respectively. There is a good agreement between **4a** and the experimental EAS of $C_{60}H_4$, in which a sharp band between 410 nm and 420 nm is present (see Figure S14). But, there is a small mismatch between 500 nm and 450 nm probably due to the missing bands from the other isomers.[25,27] All the neutral molecules display bands that emerge in the visible spectrum or its close vicinity. However, the cationic counterparts are particularly intriguing. Similar to the $C_{60}H_2^+$ cations, the $C_{60}H_4^+$ isomers also show remarkably long wavelengths for their first electronic transitions. For instance, **4i-c** and **4j-c** show weak transitions with energies smaller than 4000 nm (0.31 eV). Additionally, all the other cations within this group display allowed excitations above 2100 nm (below 0.59 eV), with the exception of **4c-c**.

3.4 Discussion

The detailed description of the spectroscopic behavior of fulleranes has been provided in Sections 3.2 and 3.3. In this section, we summarize and contextualize our results in the context of the detectability of fulleranes and their similarities and differences with PAHs, which is the main carbon-bearing family of molecules in PDRs.[5]

The IR spectral fingerprint of fulleranes is particularly sensitive to the charge state, as shown in Section 3.2. This is remarkably similar to the situation found for PAHs.[68–72] In PAHs, it is recognized that the 7.7 μm band originates from large cationic PAHs. For charged and neutral fulleranes, the main spectral difference we found is the significant decrease in intensity of the low-frequency bands between 19–16 μm and a consequential increase in the 9–6.5 μm bands. The latter range includes the 7.7 μm band probing charged PAHs, making it difficult to disentangle the contribution from fulleranes and charged PAHs. Our theoretical calculations estimate that most fulleranes must be ionized in

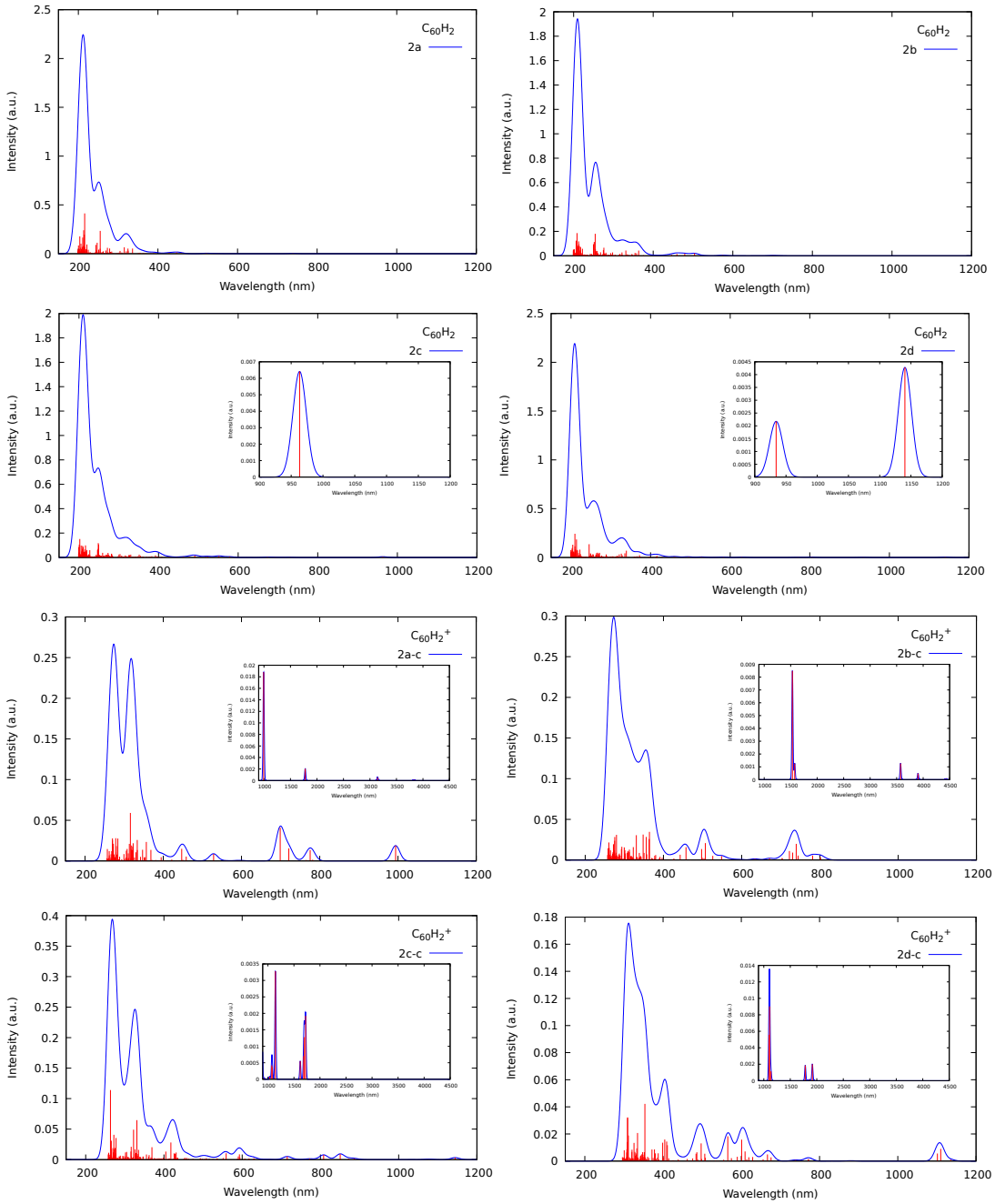

Fig. 6 Simulated electronic absorption spectra of $C_{60}H_2$ and $C_{60}H_2^+$ at the r^{2}SCAN/def2-TZVP level of theory.

PDRs, owing to the low IP, in all cases below that of C_{60}. In general, C–H functionalization in fulleranes reduces the ionization potential between 0.60 and 1.00 eV (see Table 1 for the global minimum values of each $C_{60}H_n$ and Table S9 in the SI for all relevant isomers), indicating that ionized fulleranes are expected over neutral ones. The spectral IR fingerprint of interstellar fulleranes should then be closer to that shown in the respective panels of Figures 2, 3, and 5. Still, we do not find IR spectra to be a reliable detection tool for fulleranes because of their blend with characteristic PAH frequencies. The C–H stretching region, with the spectra shown in the SI, is rather uninformative, with vibrational modes at $\sim$ 2800-2900 cm^{-1}, e.g., mixing with those of PAHs and the much more abundant CH_3 and CH_2 symmetric and asymmetric stretches found for hydrogenated amorphous carbon, an abundant constituent of cosmic dust.[73]

The spectral similarity between PAHs and fulleranes is maintained in the UV spectra presented in this work. Therefore, we do not expect UV-Vis to be a reliable detection tool for fulleranes either. However, in this work, we have extended the spectral range under study to encompass electronic transitions in the

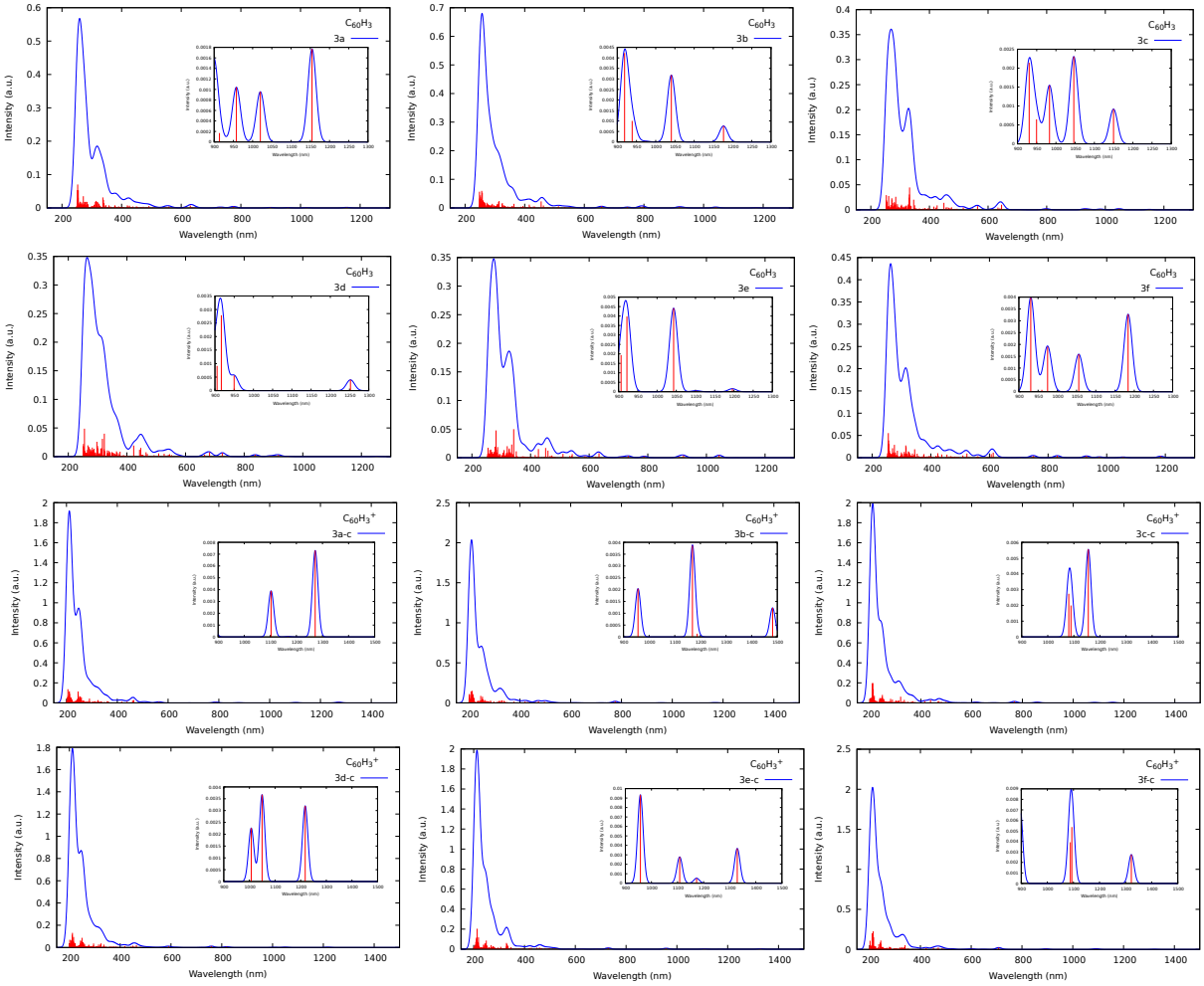

Fig. 7 Simulated electronic absorption spectra of $C_{60}H_3$ and $C_{60}H_3^+$ at the r^{2}SCAN/def2-TZVP level of theory.

near-infrared, characteristic of DIBs. Our study reveals that near-infrared features for fulleranes are very sensitive to the hydrogen position and charge state and can be used as fingerprints for the individual decomposition of interstellar fulleranes. Certainly, our DFT predictions are qualitative. We encourage further experiments to study this spectral window, producing abundant data that can be conducive to new interstellar detections. Specifically, we observe that for an even number of hydrogens in the structure, DIBs are inhibited, both for $n = 2$ and $n = 4$ in neutral fulleranes. For $n = 2$, the high energy isomers **2c** and **2d** show electronic transitions in the NIR, but are significantly less resolved than for $C_{60}H_3$. Charged fulleranes are therefore an excellent candidate for laboratory study.

Although this work focuses on the spectroscopic characterization of fulleranes, a brief comment on their role as catalysts in the formation of H_2 is pertinent. It is recognized that small hydrogenated PAHs are the key in the formation of H_2 in PDRs.[18,19,21,74] Likewise, fulleranes should be excellent catalysts, considering that the surface area for H sticking is higher in them than in PAHs, and their resilience on PDRs. A subsequent work on the importance of fulleranes on the chemistry of PDRs, based on the structural conclusions presented in this work, will be the subject of future work by us.

4 Conclusions

In this work, an automated search for hydrogenated fullerenes was performed and several low-energy isomers of $C_{60}H_n^{q+}$ were selected for simulations of IR and UV spectra based on density functional theory calculations. Interestingly, from our results, we propose new global minimum candidates for $C_{60}H_2$ and $C_{60}H_4$ which differs from previous results[23] highlighting the importance of automated workflows for global minimum optimizations. Probably, our results are different from those obtained by Zhang and co-workers due to the fact that they generated the structures manually and applied a double-zeta basis set (pc-1). In addition to the systematic search, our results for the structures were obtained using the hybrid functional B3LYP and triple-zeta basis set, which are quite suitable for structural and IR spectra simulations. Furthermore, we report the low-energy isomers of $C_{60}H_2^+$, $C_{60}H_3$, $C_{60}H_3^+$ and $C_{60}H_4^+$.

In general, the C–H distances present small variations and the dipole moment are higher for cations than for the neutral

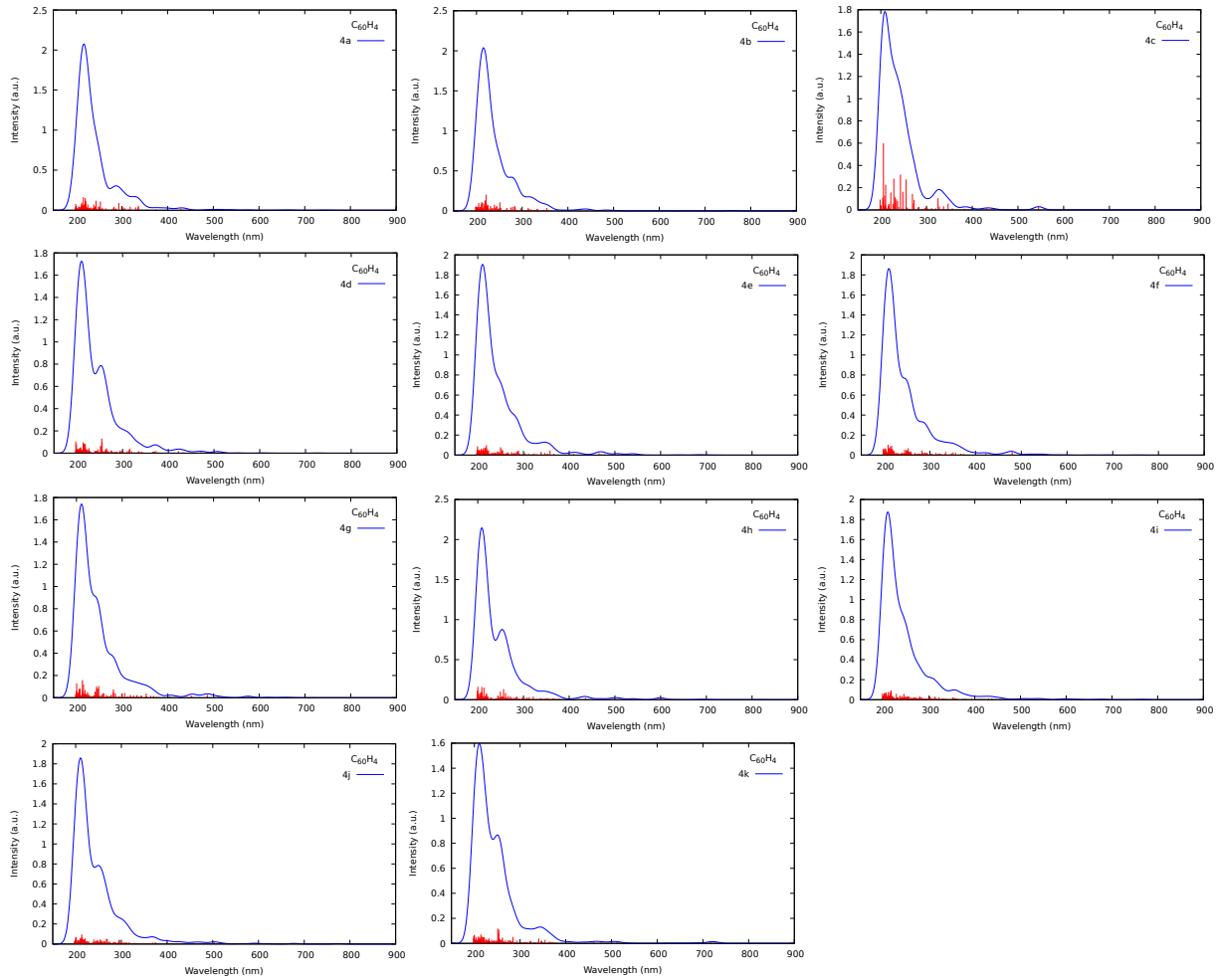

Fig. 8 Simulated electronic absorption spectra of $C_{60}H_4$ at the r^{2}SCAN/def2-TZVP level of theory.

molecules. All hydrogenated fullerenes exhibit IP smaller than the IP of C_{60} and also below the Lyman limit. Regarding PA, all hydrogenated fullerenes have higher values than C_{60} indicating that sequential hydrogenation can occur in different astronomical environments. A possible explanation for the lower IP and higher PA of hydrogenated species is that the first hydrogen addition in C_{60} causes a great strain due to the formation of sp^3 carbon atom. For the following hydrogenations, the strain effect is smaller and after the formation of $C_{60}H_{36}$, the carbon cage has a small stability.[23] Similar effects can be postulated for the IP. After the ionization of C_{60}, a great structural reorganization occurs lowering the symmetry, turning the IP of C_{60} greater than the already distorted $C_{60}H_n$ systems.

The IR spectra have similar features for neutral species as intense bands around 500–600 cm^{-1} (20.00–16.66 μm) due to cage (skeleton) deformation modes. The cation spectra exhibit additional features, particularly in the range of 1200-1600 cm^{-1} (8.33–6.25 μm), which correspond to C-C stretching and C-C-H bending modes. Consequently, cations can contribute to the 6.2 μm emission band of Unidentified Infrared Bands (UIRs). In general, the decrease in symmetry caused by hydrogenation turns the IR spectra more complex.

Remarkably, several neutral hydrogenated fullerenes exhibit electronic transitions in the near-infrared range. Exceptions are two low-energy $C_{60}H_2$ isomers and $C_{60}H_4$ species. In particular, all low-energy cations considered in this work present electronic transitions above 900 nm, indicating that these species can contribute to the DIBs. Extreme cases are some $C_{60}H_2^+$ and $C_{60}H_4^+$ isomers in which some transitions are in the 3000–4000 nm wavelength range. We hope that our work can assist fullerene cations astronomical and laboratory detections.

From an astrochemical perspective, the spectral similarity between PAHs and fulleranes makes it difficult to provide appropriate spectroscopic guidelines for the detection of the latter using (mid-infrared) MIR and UV-Vis spectroscopies. However, we found that electronic transitions in the NIR, characteristic of DIBs, act as selective fingerprints of fulleranes, in particular cationic and with an odd number of hydrogen atoms. We strongly encour-

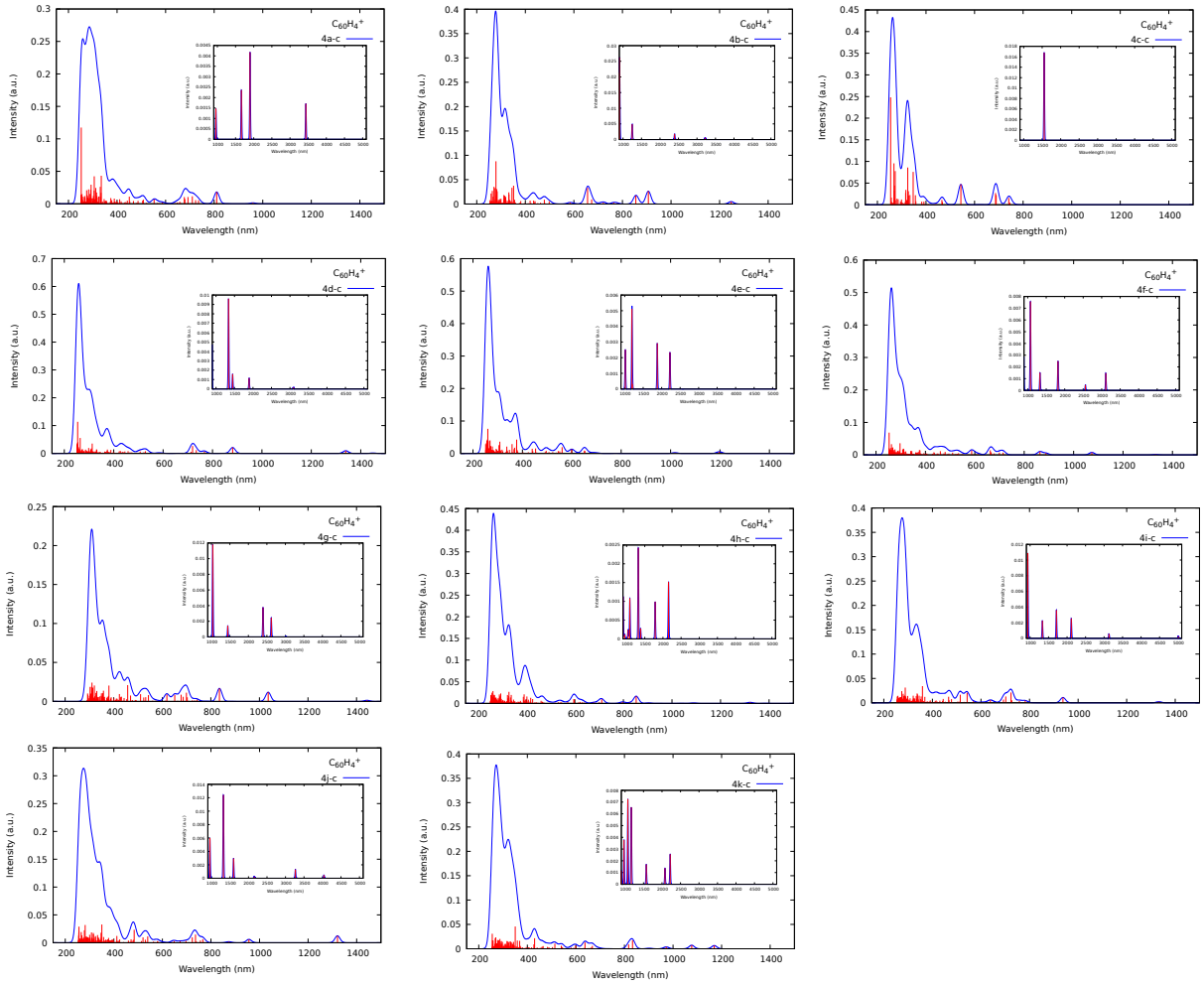

Fig. 9 Simulated electronic absorption spectra of and $C_{60}H_4^+$ at the r^{2}SCAN/def2-TZVP level of theory.

age further high-resolution investigation of these bands to build on our computational predictions.

This work serves as the beginning for an extended study of the role of fulleranes in the chemistry of the ISM.

Author Contributions

Ricardo R. Oliveira: Conceptualization, Methodology, Software, Writing - Original draft preparation, Validation, Investigation **Germán Molpeceres:** Conceptualization, Software, Writing - Original draft preparation, Investigation **Ricardo Montserrat:** Software, Writing - Original draft preparation, Investigation **Felipe Fantuzzi:** Conceptualization, Writing - Reviewing and Editing **Alexandre B. Rocha:** Resources, Writing - Review and Editing **Johannes Kästner:** Resources, Writing - Review and Editing

Conflicts of interest

There are no conflicts to declare

Acknowledgements

R.R.O. acknowledges the Conselho Nacional de Desenvolvimento Científico e Tecnológico (CNPq), Coordenação de Aperfeiçoamento Pessoal de Nível Superior (CAPES) and Fundação de Amparo à Pesquisa do Estado do Rio de Janeiro (FAPERJ) for financial support. R.R.O. and F.F. acknowledges the National Laboratory for Scientific Computing (LNCC/MCTI, Brazil) for providing HPC resources of the SDumont supercomputer, which have contributed to the research results reported within this paper (http://sdumont.lncc.br). G.M. thanks the Japan Society for the Promotion of Science (JSPS International Fellow P22013, and Grant-in-aid 22F22013) for its support. The authors acknowledge support from the state of Baden-Württemberg through bwHPC and the German Research Foundation (DFG) through grant no INST 40/575-1 FUGG (JUSTUS 2 cluster) and the Research Center for Computational Science, Okazaki, Japan (Projects: 22-IMS-C301, 23-IMS-C128).

Notes and references

1 T. P. Snow and B. J. McCall, *Annu. Rev. Astron. Astrophys.*, 2006, **44**, 367–414.

2 A. Omont, *Astron. Astrophys.*, 2016, **590**,.

3 T. R. Geballe, *Journal of Physics: Conference Series*, 2016, **728**, 062005.

4 M. L. Heger, *Lick Observatory Bulletin*, 1922, **10**, 141–145.

5 A. G. G. M. Tielens, *Molecular Astrophysics*, Cambridge University Press, Cambridge, 2021.

6 J. Zhen, P. Castellanos, D. M. Paardekooper, N. Ligterink, H. Linnartz, L. Nahon, C. Joblin and A. G. Tielens, *Astrophys. J. Lett.*, 2015, **804**, L7.

7 O. Berné and A. G. G. M. Tielens, *Proceedings of the National Academy of Science*, 2012, **109**, 401–406.

8 J. Zhen, P. Castellanos, D. M. Paardekooper, H. Linnartz and A. G. G. M. Tielens, *Astrophys. J. Lett.*, 2014, **797**, L30.

9 C. Jäger, F. Huisken, H. Mutschke, I. L. Jansa and T. Henning, *Astrophys. J.*, 2009, **696**, 706–712.

10 E. K. Campbell, M. Holz, D. Gerlich and J. P. Maier, *Nature*, 2015, **523**, 322–323.

11 J. Cami, J. Bernard-Salas, E. Peeters and S. E. Malek, *Science*, 2010, **329**, 1180–1182.

12 D. L. Lichtenberger, M. E. Jatcko, K. W. Nebesny, C. D. Ray, D. R. Huffman and L. D. Lamb, *MRS Proceedings*, 1990, **206**, 673.

13 E. Herbst, *Chem. Soc. Rev.*, 2001, **30**, 168–176.

14 E. Herbst, *J. Phys. Chem. A*, 2005, **109**, 4017–4029.

15 V. Wakelam, I. W. Smith, E. Herbst, J. Troe, W. Geppert, H. Linnartz, K. Öberg, E. Roueff, M. Agúndez, P. Pernot, H. M. Cuppen, J. C. Loison and D. Talbi, *Space Sci. Rev.*, 2010, **156**, 13–72.

16 R. C. Haddon, *Science*, 1993, **261**, 1545–1550.

17 S. Iglesias-Groth, D. A. García-Hernández, F. Cataldo and A. Manchado, *Monthly Notices of the Royal Astronomical Society*, 2012, **423**, 2868–2878.

18 T. P. Goumans and J. Kästner, *Angew. Chem. Int. Ed.*, 2010, **49**, 7350–7352.

19 T. P. Goumans, *Mon. Not. R. Astron. Soc.*, 2011, **415**, 3129–3134.

20 S. Cazaux, L. Boschman, N. Rougeau, G. Reitsma, R. Hoekstra, D. Teillet-Billy, S. Morisset, M. Spaans and T. Schlathölter, *Sci. Rep.*, 2016, **6**, 19835.

21 N. Foley, S. Cazaux, D. Egorov, L. M. Boschman, R. Hoekstra and T. Schlathölter, *Mon. Not. R. Astron. Soc.*, 2018, **479**, 649–656.

22 S. Cazaux, Y. Arribard, D. Egorov, J. Palotás, R. Hoekstra, G. Berden, J. Oomens and T. Schlathölter, *Astrophys. J.*, 2019, **875**, 27.

23 Y. Zhang, S. Sadjadi, C.-H. Hsia and S. Kwok, *The Astrophysical Journal*, 2017, **845**, 76.

24 C. C. Henderson and P. A. Cahill, *Science*, 1993, **259**, 1885–1887.

25 R. Bensasson, E. Bienvenue, J.-M. Janot, S. Leach, P. Seta, D. Schuster, S. Wilson and H. Zhao, *Chemical Physics Letters*, 1995, **245**, 566–570.

26 A. Webster, *Monthly Notices of the Royal Astronomical Society*, 1993, **263**, L55–L58.

27 A. Webster, *Monthly Notices of the Royal Astronomical Society*, 1997, **288**, 221–224.

28 E. F. Sheka, *Journal of Molecular Modeling*, 2011, **17**, 1973–1984.

29 A. Vats and A. Pathak, *Journal of Astrophysics and Astronomy*, 2023, **44**, 32.

30 K. Tokunaga, S. Ohmori, H. Kawabata and K. Matsushige, *Japanese Journal of Applied Physics*, 2008, **47**, 1089.

31 L. B. Tuli, S. J. Goettl, A. M. Turner, A. H. Howlader, P. Hemberger, S. F. Wnuk, T. Guo, A. M. Mebel and R. I. Kaiser, *Nature Communications*, 2023, **14**, 1527.

32 P. Pracht, C. A. Bauer and S. Grimme, *Journal of Computational Chemistry*, 2017, **38**, 2618–2631.

33 Y. Tanuma, T. Maekawa and C. Ewels, *Crystals*, 2021, **11**, 1334.

34 P. Schwerdtfeger, L. Wirz and J. Avery, *Journal of Computational Chemistry*, 2013, **34**, 1508–1526.

35 A. O. Lykhin, S. Ahmadvand and S. A. Varganov, *Journal of Physical Chemistry Letters*, 2019, **10**, 115–120.

36 C. Lee, W. Yang and R. G. Parr, *Phys. Rev. B*, 1988, **37**, 785–789.

37 A. D. Becke, *J. Chem. Phys.*, 1993, **98**, 5648–5652.

38 S. Grimme, J. Antony, S. Ehrlich and H. Krieg, *J. Chem. Phys.*, 2010, **132**, 154104.

39 S. Grimme, S. Ehrlich and L. Goerigk, *J. Comput. Chem.*, 2011, **32**, 1456–1465.

40 F. Weigend and R. Ahlrichs, *Phys. Chem. Chem. Phys.*, 2005, **7**, 3297.

41 M. Ernzerhof and G. E. Scuseria, *J. Chem. Phys.*, 1999, **110**, 5029–5036.

42 C. Adamo and V. Barone, *J. Chem. Phys.*, 1999, **110**, 6158–6170.

43 T. Yanai, D. P. Tew and N. C. Handy, *Chemical Physics Letters*, 2004, **393**, 51–57.

44 J.-D. Chai and M. Head-Gordon, *Phys. Chem. Chem. Phys.*, 2008, **10**, 6615.

45 J. P. Perdew, A. Ruzsinszky, G. I. Csonka, L. A. Constantin and J. Sun, *Phys. Rev. Lett.*, 2009, **103**, 026403.

46 J. W. Furness, A. D. Kaplan, J. Ning, J. P. Perdew and J. Sun, *The Journal of Physical Chemistry Letters*, 2020, **11**, 8208–8215.

47 J. C. Santos, F. Fantuzzi, H. M. Quitián-Lara, Y. Martins-Franco, K. Menéndez-Delmestre, H. M. Boechat-Roberty and R. R. Oliveira, *Monthly Notices of the Royal Astronomical Society*, 2022, **512**, 4669–4682.

48 C. Suellen, R. G. Freitas, P.-F. Loos and D. Jacquemin, *Journal of Chemical Theory and Computation*, 2019, **15**, 4581–4590.

49 J. Kaur, E. Ospadov and V. N. Staroverov, *Journal of Chemical Theory and Computation*, 2019, **15**, 4956–4964.

50 M. K. Kesharwani, B. Brauer and J. M. L. Martin, *The Journal*

of Physical Chemistry A, 2015, **119**, 1701–1714.

51 S. W. McElvany, M. M. Ross and J. H. Callahan, *Accounts of Chemical Research*, 1992, **25**, 162–168.

52 P. Pracht, R. Wilcken, A. Udvarhelyi, S. Rodde and S. Grimme, *Journal of Computer-Aided Molecular Design*, 2018, **32**, 1139–1149.

53 P. Pracht and S. Grimme, *Journal of Physical Chemistry A*, 2021, **125**, 5681–5692.

54 P. Pracht, F. Bohle and S. Grimme, *Physical Chemistry Chemical Physics*, 2020, **22**, 7169–7192.

55 C. Bannwarth, S. Ehlert and S. Grimme, *Journal of Chemical Theory and Computation*, 2019, **15**, 1652–1671.

56 S. Grimme, J. G. Brandenburg, C. Bannwarth and A. Hansen, *The Journal of Chemical Physics*, 2015, **143**, 054107.

57 J. J. Fifen, Z. Dhaouadi and M. Nsangou, *J. Phys. Chem. A*, 2014, **118**, 11090–11097.

58 R. R. Oliveira, G. Molpeceres, F. Fantuzzi, H. M. Quitián-Lara, H. M. Boechat-Roberty and J. Kästner, *Monthly Notices of the Royal Astronomical Society*, 2021, **500**, 2564–2576.

59 F. Neese, F. Wennmohs, U. Becker and C. Riplinger, *J. Chem. Phys.*, 2020, **152**, 224108.

60 K. Yamamoto, M. Saunders, A. Khong, R. J. Cross, M. Grayson, M. L. Gross, A. F. Benedetto and R. B. Weisman, *Journal of the American Chemical Society*, 1999, **121**, 1591–1596.

61 V. Schettino, M. Pagliai, L. Ciabini and G. Cardini, *The Journal of Physical Chemistry A*, 2001, **105**, 11192–11196.

62 J. Palotás, J. Martens, G. Berden and J. Oomens, *Nature Astronomy*, 2020, **4**, 240–245.

63 D. Strelnikov, B. Kern and M. M. Kappes, *Astronomy & Astrophysics*, 2015, **584**, A55.

64 D. Gerlich, J. Jašík, D. V. Strelnikov and J. Roithová, *The Astrophysical Journal*, 2018, **864**, 62.

65 C. R. Stoldt, R. Maboudian and C. Carraro, *The Astrophysical Journal*, 2001, **548**, L225–L228.

66 S. Leach, M. Vervloet, A. Desprès, E. Bréheret, J. P. Hare, T. John Dennis, H. W. Kroto, R. Taylor and D. R. Walton, *Chemical Physics*, 1992, **160**, 451–466.

67 J. Soler, R. Sarkar and M. Boggio-Pasqua, *The Journal of Physical Chemistry A*, 2019, **123**, 1824–1829.

68 F. Galliano, S. C. Madden, A. G. G. M. Tielens, E. Peeters and A. P. Jones, *Astrophys. J.*, 2008, **679**, 310–345.

69 C. Boersma, J. Bregman and L. J. Allamandola, *Astrophys. J.*, 2018, **858**, 67.

70 A. Maragkoudakis, E. Peeters and A. Ricca, *Mon. Not. R. Astron. Soc.*, 2020, **494**, 642–664.

71 B. T. Draine, A. Li, B. S. Hensley, L. K. Hunt, K. Sandstrom and J. D. T. Smith, *Astrophys. J.*, 2021, **917**, 3.

72 J. Chastenet, J. Sutter, K. Sandstrom, F. Belfiore, O. V. Egorov, K. L. Larson, A. K. Leroy, D. Liu, E. Rosolowsky, D. A. Thilker, E. J. Watkins, T. G. Williams, A. T. Barnes, F. Bigiel, M. Boquien, M. Chevance, D. A. Dale, J. M. D. Kruijssen, E. Emsellem, K. Grasha, B. Groves, H. Hassani, A. Hughes, K. Kreckel, S. E. Meidt, H.-A. Pan, M. Querejeta, E. Schinnerer and C. M. Whitcomb, *The Astrophysical Journal Letters*, 2023, **944**, L12.

73 G. Molpeceres, V. Timón, M. Jiménez-Redondo, R. Escribano, B. Maté, I. Tanarro and V. J. Herrero, *Physical Chemistry Chemical Physics*, 2017, **19**, 1352–1360.

74 S. Cazaux, L. Boschman, N. Rougeau, G. Reitsma, R. Hoekstra, D. Teillet-Billy, S. Morisset, M. Spaans and T. Schlathölter, *Scientific Reports*, 2016, **6**, 19835.